

Plant-Inspired Soft Bistable Structures Based on Hygroscopic Electrospun Nanofibers

Dario Lunni,* Matteo Cianchetti, Carlo Filippeschi, Edoardo Sinibaldi,* and Barbara Mazzolai*

The tissue composition and microstructures of plants have dynamic morphologies that change according to their environments. Recently, multifunctional responsive materials and smart structures also took inspiration from these plants' features. *Dionaea muscipula* leaves provide a remarkable example of an optimized structure that, owing to the synergistic integration of bistability, material, and geometrical properties, permits to overcome the performance limits of purely diffusive processes. In this paper, a hygroscopic bistable structure (HBS) inspired by the Venus flytrap leaves is presented, obtained by bonding prestretched poly(dimethylsiloxane) (PDMS) layers prior to depositing electrospun polyethylene oxide (PEO) nanofibers. A hygroresponsive bilayer (HBL) is also obtained by electrospinning of PEO on an unstretched PDMS layer. The hygroscopic material (Young's modulus and hygroscopic expansion) is mechanically characterized so as to predict the response time of a bending HBL in response to a step humidity variation. The HBS response time (≈ 1 s) is sensibly lower than the one of purely diffusive HBL (≈ 10 s) thanks to bistability. An illustrative implementation is also presented, exploiting an HBS to trigger the curvature of a PDMS optical focusing system. The developed plant-inspired soft bistable structure can also be used for sensing (e.g., humidity), energy harvesting, as well as advanced soft robotics applications.

The synergetic integration of advanced materials and smart structures opens the way to new methodologies for designing systems as a whole with optimized functionality and flexibility. In this perspective, smart materials are of great interest in many fields like architecture, micro-robotics, and soft robotics,^[1] where actuation and sensing mechanisms are often highly integrated with the robot body and functionality.^[2] Among smart materials, environmental responsive materials could help to solve problems related to energy efficiency and structure adaptation thanks to the ability to convert environmental changes in mechanical energy used for self-propulsion or reconfiguration. The activation principles of environmental responsive materials can be based on heat,^[3] light,^[4,5] or chemical concentration,^[6] and recently strong interest has been demonstrated for moisture responsive materials.

One of the most common materials used in hygroresponsive systems is cellulose paper, thanks to its swelling properties when the moisture level is increased.


When coupled with an inert substrate in a bilayer system, this material can lead to the bending of the structure in a predefined direction.^[7] Many artificial polymers have been synthesized^[8,9] and also biological materials have been used as materials sensitive to humidity.^[10] Often, hygroresponsivity has been coupled to temperature control, leading to hygromorphic thermoresponsive systems controllable using near-infrared (NIR) light^[11] or Joule effect.^[12] To improve the response time of these systems (increasing the diffusivity of the membrane), also woven electrospun nanofibers (NFs) membrane has been synthesized, easing the diffusion of environmental moisture in the active layer and improving the directionality of the actuation.^[13]

Nevertheless, many open issues remain regarding the effective implementation of hygromorphic materials in soft structures. First, accurate studies of the mechanical properties and models to describe these materials and structures are not trivial. Second, the response of these systems remains constrained by the poroelastic limit of the constitutive material, namely, the diffusive properties. This aspect strongly limits the practical usability of hygromorphic materials.

D. Lunni, C. Filippeschi, Dr. E. Sinibaldi, Dr. B. Mazzolai
Center for Micro-BioRobotics
Istituto Italiano di Tecnologia
Viale Rinaldo Piaggio 34, Pontedera, Pisa 56025, Italy
E-mail: dario.lunni@iit.it; edoardo.sinibaldi@iit.it; barbara.mazzolai@iit.it

D. Lunni, Dr. M. Cianchetti
The BioRobotics Institute
Scuola Superiore Sant'Anna
Viale Rinaldo Piaggio 34, Pontedera, Pisa 56025, Italy

D. Lunni, Dr. M. Cianchetti
Department of Excellence in Robotics & AI
Scuola Superiore Sant'Anna
Piazza Martiri della Libertà 33, Pisa 56127, Italy

 The ORCID identification number(s) for the author(s) of this article can be found under <https://doi.org/10.1002/admi.201901310>.

© 2020 The Authors. Published by WILEY-VCH Verlag GmbH & Co. KGaA, Weinheim. This is an open access article under the terms of the Creative Commons Attribution License, which permits use, distribution and reproduction in any medium, provided the original work is properly cited.

The copyright line for this article was changed on 23 January 2020 after original online publication.

DOI: 10.1002/admi.201901310

A key example of synergetic integration of moisture responsive materials in smart structures, achieving performances that are not constrained by the poroelastic limit, is given by plant kingdom.^[14] Plant movements gained much attention from an engineering point of view for their high energy efficiency and adaptability, and for the ability to exploit different environmental conditions.^[15] Most of the botanical movements are driven by osmosis principles^[16] through vegetal tissues, whose mechanical and poroelastic properties affect the direction and the dynamics allowing the generation of many different kind of deformations.^[14] Anisotropic swelling of tissues allows, for instance, opening and closure of pine cones^[17] or movements of the wild wheat,^[18] but also more complex deformations like twisting and coiling can be achieved.^[16] Nevertheless, some impressive examples of rapid movements, unconstrained from poroelastic limits, are fundamental for plants survival like seed dispersal (*Hura crepitans*),^[18] defense (*Mimosa pudica*),^[19] and nutrition (*Aldrovanda vesiculosa*).^[20] Among the others, the Venus flytrap (*Dionaea muscipula*) closing mechanism, which can shut the leaf in a fraction of second, fascinated scientists since the time of Charles Darwin.^[21] These examples of rapid movements rely on the accumulation of elastic energy, led by swelling and shrinkage, that is released by snap-buckling^[22] or explosive mechanisms.^[23]

Herein, we present a hygroscopic bistable sheet (HBS) that couples the hygromorphic capability of electrospun material with the mechanical advantage of preloaded structure to improve the actuation speed. As the carnivorous plant *D. muscipula* exploits a snap-buckling mechanism, we implement a snap mechanism coupled with a hygroresponsive membrane to amplify the speed of closure. We model the mechano/diffusive behavior of non-bistable hygromorphic bilayer (HBL) to quantitatively assess the response time of such purely diffusive mechanisms and compare it to the snapping ones. At last, for the sake of illustration, we implement the whole system in an optical device able to focus light depending on environmental conditions.

The most frequent explanation given for the extraordinary rapid movement of the Venus flytrap is that the plant exploits the release of elastic energy stored in the structure during the opening.^[22] This storage of elastic energy takes place thanks to the particular geometry of the leaf that is characterized by two inverted curvatures: curved outward (convex) in the open state (Figure 1a) and curved inward (concave) in the closed state^[21] (Figure 1b). For double-curved shells, the bending and stretching modes of deformations are coupled, meaning that bending causes the leaf to be also stretched, and vice versa.^[24] Such behavior is associated with a prestretch in the structure, which can be observed by cutting thin strips of leaf in the two main directions of the curvature. These thin strips cut from the leaf naturally bend in planes orthogonal to each other, supporting the nature of the underlying bistable mechanism (Figure 1b, insets). To better understand the strain distribution in the leaf we analyzed its microstructure. Using polarized light microscopy, we investigated the presence of reinforcing microfibrils^[25] in the leaf structure. In thin sections of the leaf cut parallel to the midrib (the large vein along the midline of the leaf), the circular cell walls of the tissue shine brightly, and the upper epidermis is brighter than the lower one (Figure 1c,d).

This indicates the presence of microfibrils reinforcing azimuthally the cylindrical cell wall of the tissue and, as a consequence, the tissue is more extensible in the direction of the cells' axis. In the thin sections cut perpendicular to the midrib, the upper epidermis of the leaf shines brightly indicating the presence of microfibrils running perpendicular to the midrib (Figure 1e). These observations related to the internal structure of the leaf are confirmed by the analysis of the strain on the upper and lower epidermis of the leaf,^[26] confirming the hypothesis that the external layers of the leaf are under expansion during the snapping motion. The leaf structure characterized by a preferential deformation layer during the snapping motion inspired us to design HBS (Figure 1f,g), namely, a snapping mechanism that can be triggered when the humidity level varies, and we compared the performance of this structure with the performance of non-bistable HBL.

Both HBS and HBL are composed of a passive layer of poly(dimethylsiloxane) (PDMS) and a hygroscopic active layer based on polyethylene oxide (PEO) electrospun NFs. PDMS was selected as passive layer for its elasticity, humidity inertness and optical properties. Second, PDMS layers have the possibility to be permanently bonded together through surface plasma treatment activation, allowing the development of a simple process to bond prestretched sheets. PEO was selected as active material because of its well-known high sensitivity to the moisture level of the environment,^[27] swelling in response to a rise of environmental humidity. The sensitivity of PEO to the concentration of water molecules in air can be improved when deposited as a membrane of nanofibers.^[13] Aligned PEO-NF can be produced through electrospinning using a rotating collector. A schematic representation of the manufacturing process of HBL and HBS is represented in Figure 2a (see also the Experimental Section). We developed a highly customizable process to fabricate our structures thanks to the use of spin coating, laser cutting, and electrospinning techniques.

Spin coating and laser cutting techniques allow achieving an accurate control on the PDMS thickness and shape of the layer. After the curing and cutting process, the spin-coated PDMS layers can be easily peeled off from the silicon wafer, thanks to the silanization, and prepared for the NF deposition. To build up simple HBL, we attach a PDMS layer to a rotating collector and collect aligned NF through electrospinning. Alternatively, to build up HBS, we start from the cut of two PDMS layers and impose a uniaxial prestretch ϵ_d using a customized setup composed of micrometric sliders. Then, exploiting plasma treatment activation of the PDMS surfaces, we bond the prestretched layers keeping the stretched directions orthogonal to each other.^[28] Through this process, we can obtain a BS. In particular, the behavior of such sheet depends on the adimensional parameter $\tilde{w} = w\sqrt{k_0/h}$, where w is the width of the sheet, k_0 is the curvature of thin strips cut from the sheet along the principal curvature, and h is the sheet thickness. This adimensional parameter describes the ratio between the stretching and bending terms of the elastic energy of the sheet. The phenomenon of mechanical bistability manifests when the elastic energy of the structure is dominated by the stretching terms, i.e., when $\tilde{w} \gg 1$.^[24] In the last fabrication step, the BS is used as substrate for the electrospinning process, attaching it on the rotating collector of the electrospinning, obtaining the HBS.

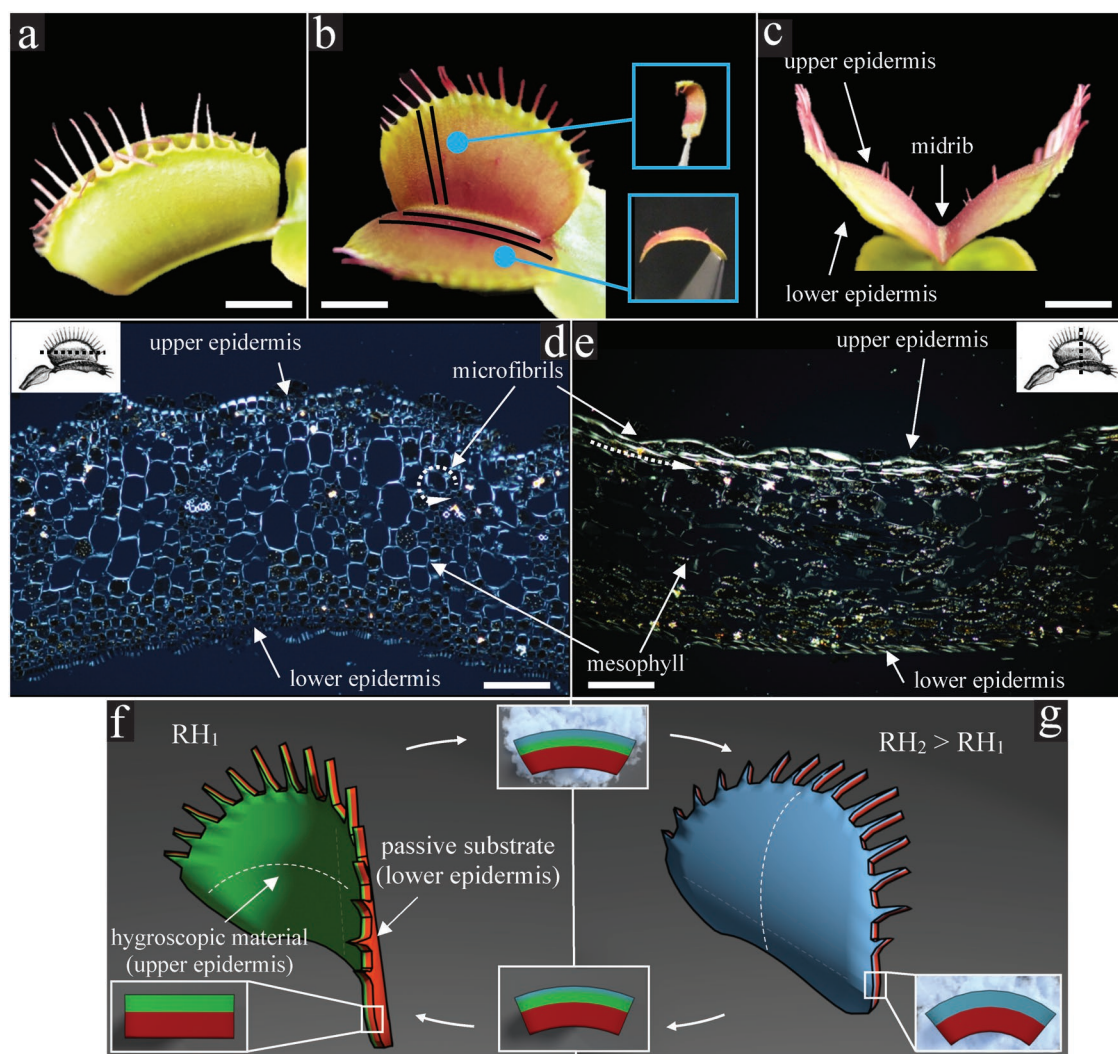


Figure 1. Venus flytrap (*Dionaea muscipula*) leaf in its a) closed and b) open configuration (scale bar: 1 cm). Inset: upon cutting along the cut lines (overlay), perpendicular to and parallel to the leaf midrib, the leaf strips spontaneously bend in planes orthogonal to each other, owing to the bistable character of the leaf structure. c) Venus flytrap leaf in its open configuration (side view), showing in particular upper and lower epidermis. d) Polarized microscope image of a leaf cut section parallel to the midrib (see inset). e) Polarized microscope image of a leaf cut section perpendicular to the midrib (see inset). In both (d) and (e), the upper epidermis shines brighter than the lower epidermis and mesophyll owing to the higher density of reinforcing microfibrils, which run perpendicular to the section plane (scale bar: 150 μm). Schematic of artificial Venus flytrap leaf (AVFL) in its f) open and g) closed configuration. It is based on a bistable bilayer: a passive substrate as artificial lower epidermis; a hygroscopic layer made of electrospun nanofibers as artificial upper epidermis, which triggers the transition between the two stable configurations upon swelling/deswelling (see insets).

NF are collected aligned and parallel to one of the two planes that contain the bending curvature of the structure, in this way, when activated, the swelling of the fibers allows the system to reduce the mean curvature until snapping.

The opposite curvatures of thin strips cut from a Venus flytrap leaf can be compared to the deformations of thin strips cut along the directions of the main curvatures of the HBS. Likewise the natural strips, artificial ones bend in planes orthogonal to each other with curvature radius $r_s (= 1/k_0)$ (Figure 2b). Controlling the symmetric prestretch ε_d of the two bonded PDMS layers, it is possible to predict the curvature radius r of the stable states of the BS. The radius of curvature of thin strips cut along the principal direction of curvature of the BS can be analyzed to predict the final shape. The Timoshenko bilayer

theory^[29] is applied to these strips considering the stress caused by the imposed prestretched condition, obtaining the radius of curvature r_s normalized with respect to their thickness h (see the Supporting Information). Following the approach used by Armon et al.,^[24] the normalized radius of curvature r/h of BS can be predicted (Figure 2c).

The mechanical and morphological properties of PEO nanofibers membrane were studied to predict and compare the performance of bistable and non-bistable systems that use PEO-NF as integrated actuator. At the end of the electrospinning process, the PEO membrane can be removed from the collector and analyzed. The scanning electron microscope (SEM) image of the PEO membrane shows the nanofibers (Figure 2d). Although not perfectly aligned, more than 85% of the fibers

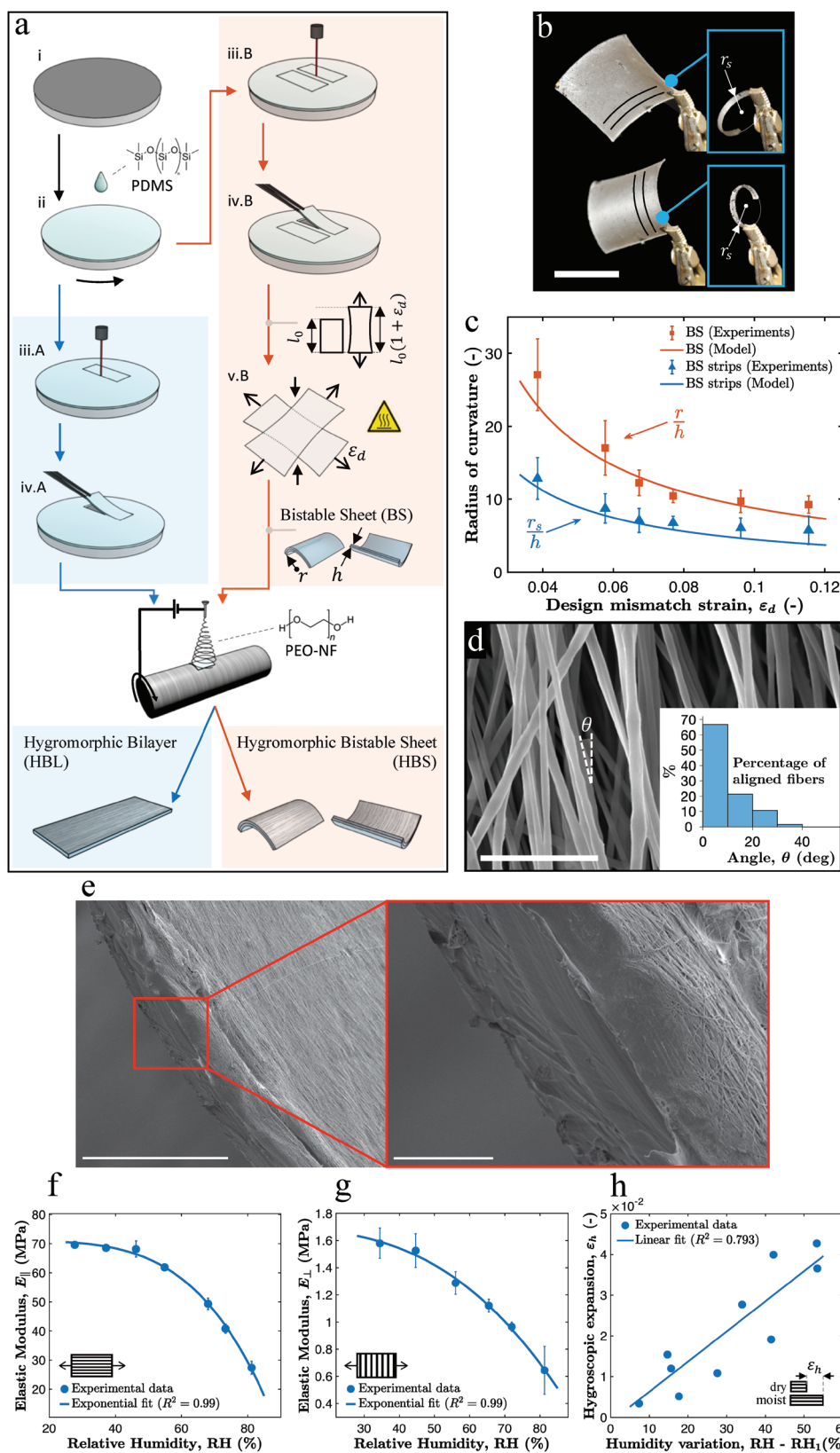


Figure 2. a) Manufacturing process (schematic) to obtain a hygromorphic bilayer (HBL) or a hygromorphic bistable sheet (HBS). Process starts with i) silanization of a silicon wafer, ii) deposition of a PDMS layer by spin coating. To obtain an HBL, iii.A) a rectangular PDMS layer is laser cut and iv.A) peeled off. By electrospinning of PEO nanofibers (NF) on the PDMS layer attached to a rotating collector, the HBL is finally obtained. Alternatively,

has a misalignment of less than 20° (Figure 2d inset). Cross-section of HBL showing the adhesion between PEO-NF and PDMS layers is depicted in Figure 2e: no delamination was observed during HBL deformation, not even when varying the relative humidity (RH) over a high number of cycles as shown in Figure 3. Adhesion is also preserved when cutting (using sharp cutter) the composite, as shown in Figure 2e. To predict the mechanical behavior of the bilayers when activated by humidity changes, we carried out tensile tests to characterize the Young's modulus of the PEO membrane alone. Because of the effect of moisture on the mechanical properties of the material, the tests were performed in a climatic chamber at different level of RH at fixed temperature (25°C). Also weight variation of PEO caused by RH variation has been investigated (see 1 in the Supporting Information). The material shows a decay of the stiffness with the increase of the RH level in both the directions parallel and perpendicular to the average fibers' axis (Figure 2f,g). The dependence of the mechanical properties on the RH level can be described with a power law (see the Supporting Information). As expected, the mechanical properties of the membrane are strongly anisotropic because of the preferential orientation of the nanofibers. The Young's modulus measured in the direction parallel to the average fiber axis turns out to be sensibly higher than the one measured in the orthogonal direction. Using the same setup, we measured the dependence of the expansion of the material with respect to the RH level (see the Experimental Section), which can be fit with a linear trend whose slope corresponds to the hygroscopic expansion coefficient α (Figure 2h; see also the Supporting Information).

Considering the above characterization, we investigated the dynamic performance of a HBL (PEO/PDMS) in response to a sudden change of the RH level. We induced the sudden change in the RH level exposing a source of water in proximity of the HBL and measuring the initial (RH_1) and the final (RH_2) level of RH in proximity of the bilayer, kept in a closed controlled environment. The variation of the RH level in the environment causes the swelling of the PEO-NF. The coupling between the hygroscopic material (PEO-NF) and the passive one (PDMS) leads to a variation in curvature of the structure (as illustrated in Figure 3a).

Considering the diffusive nature of the movement of water molecules through the PEO membrane, the variation of the RH level in the PEO active membrane can be described using a 1D diffusion equation $\partial\phi/\partial t = D \partial^2\phi/\partial z^2$ where $\phi(z, t)$ is the concentration of water molecules, t is time, D is the diffusivity of the membrane, and z is the coordinate along the thickness of the active layer positioned as depicted in Figure 3b. Considering

the appropriate boundary conditions, the equation can be solved analytically (see the Supporting Information). The scalar field $\phi(z, t)$, obtained by solving the diffusion equation, can be used to describe the distribution of the hygroscopic strain and the variation of the Young's modulus of the material using the previous experimental trends. Moreover, recalling the equations describing the static equilibrium of forces and moments on the structure,^[30] the bilayer curvature κ can be numerically predicted by explicit mathematical model (see the Supporting Information). Once reached a steady-state condition, the bilayer curvature κ , dependent on the RH level, is compared with the predicted one (Figure 3c).

Considering the solution $\phi(z, t)$ at each time step, also a quasi-static approach can be considered to describe the time-dependent curvature variation, in which the only calibrated parameter of the model is the diffusivity D that depends on the membrane porosity. In particular, we obtain D (equal to $1.5 \cdot 10^{-10} \text{ m s}^{-2}$) fitting the dynamic variation of curvature as function of time for the bilayers with NF thickness (h_{NF}) equal to $30 \mu\text{m}$ and predict the dynamics of the bilayer with $h_{\text{NF}} = 60 \mu\text{m}$ (Figure 3d). Increasing the thickness, the saturation time increases because of the longer time required by the water molecules to saturate the active layer. The reliability of HBL is tested with repeated RH level variation cycles without showing a remarkable degradation of the bilayer performance (Figure 3e). The absence of interfacial stripping after usage is also investigated through cross-section SEM images (2, Supporting Information).

To compare the performance of a HBL with the performance of a system characterized by bistability, we cut an HBS with a morphometry similar to that one of a real Venus flytrap leaf, obtaining a system here called artificial Venus flytrap leaf (AVFL) (Figure 3f). Taking in consideration the mean curvature variation of the bistable system, the actuation time of the AVFL results to be less than 1 s when exposed to a sudden RH level variation (Figure 3g). The time scale of the movement τ of the AVFL results to be an order of magnitude smaller than the actuation time of the HBL for the same active layer thickness (Figure 3h). The structural properties of AVFL allow the improvement of the reaction time thanks to the storage of the elastic energy in the elastically incompatible structure. As the natural counterpart, our system can overcome the velocity limits imposed by the diffusion of the water molecules in the active tissues (poroelastic limit). Comparing the reaction time as function of the active dimension in the plant kingdom and in the artificial systems, we can trace the poroelastic limits of the systems and see how the bistability allows, in both cases, to overcome these limits (Figure 3h). This actuation speed

to obtain an HBS, iii.B) two PDMS layers are cut, iv.B) peeled off, and v.B) suitably rotated, prestretched (ϵ_d denoting the mismatch strain), and plasma bonded to obtain a bistable sheet (BS) with thickness (h) and radius of curvature (r). By electrospinning of PEO nanofibers (PEO-NF) on the BS attached to a rotating collector, an HBS is finally obtained. b) BS stable configurations (scale bar: 1 cm). Upon cutting along the cut lines (overlay), the obtained strips spontaneously bend with curvature radius r_s in orthogonal planes (insets). c) Normalized radius of curvature for the entire BS (r/h) and for cut thin strips (r_s/h), as function of the mismatch strain (ϵ_d) imposed during the manufacturing process. Both experimental data and model predictions are shown. d) Scanning electron microscopy (SEM) image of the NF layer (scale bar: $2 \mu\text{m}$) on a PDMS substrate showing a high degree of alignment (inset). e) Cross-section of the obtained HBL (scale bar: $300 \mu\text{m}$) showing the interface between active and passive layer (inset, scale bar: $50 \mu\text{m}$). Characterization of the PEO-NF membrane: f) elastic modulus measured in the direction parallel to the average fiber axis (maximum standard deviation $<6 \text{ MPa}$), g) elastic modulus measured in direction perpendicular to the average fiber axis, and h) hygroscopic expansion in the direction parallel to the average fiber axis (the slope of the fit provides the hygroscopic expansion coefficient $\alpha = 0.076$).

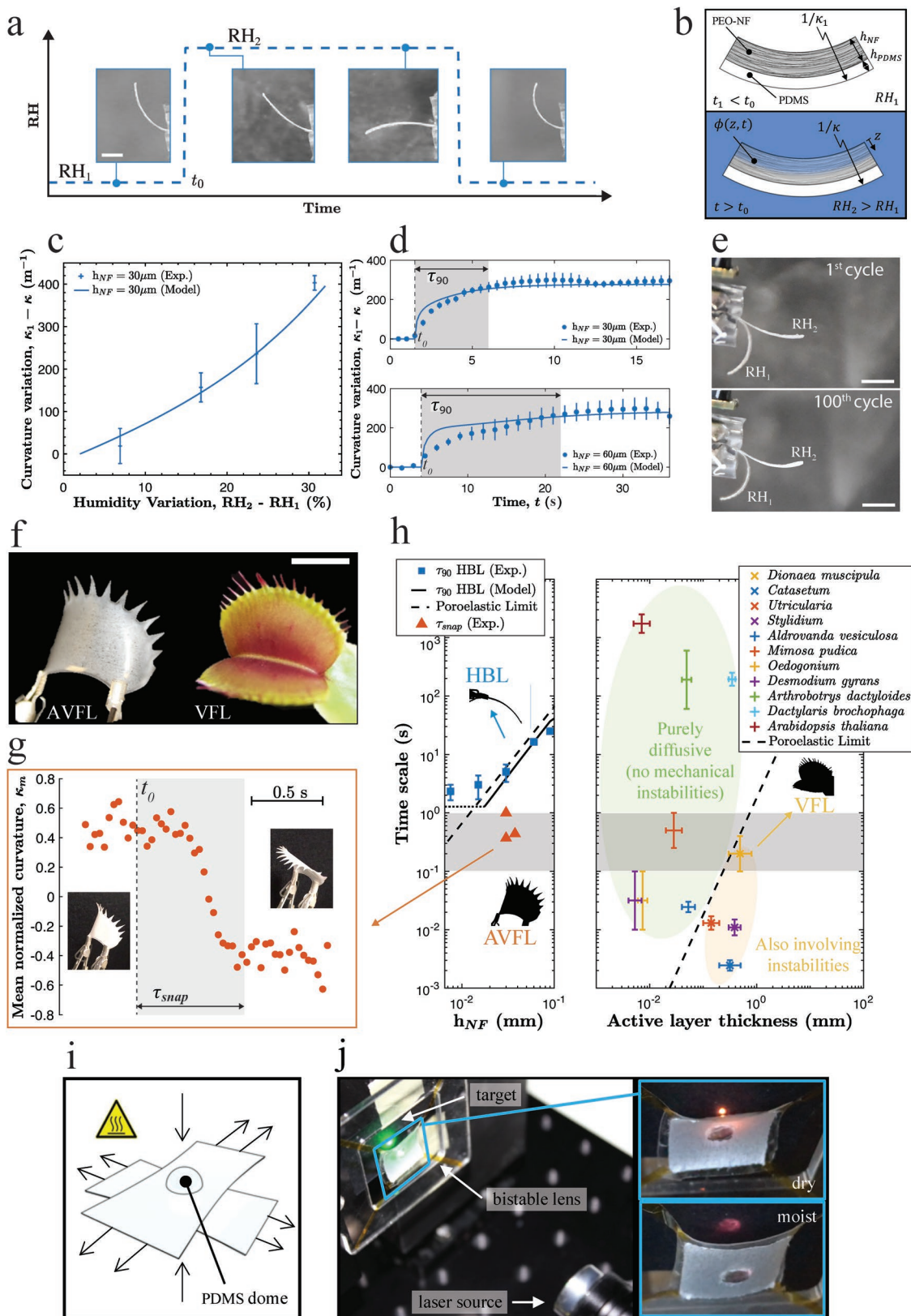


Figure 3. a) Response of HBL to a step variation of relative humidity (from RH₁ to RH₂, scale bar: 3 mm). b) HBL schematic used for modeling water diffusion. The model predicts the change in curvature (κ) as a function of a change in RH occurring at time t_0 , by determining the water concentration $\phi(z, t)$ within the NF membrane ($z \in [0; h_{NF}]$) at time t . c) Steady-state curvature variation versus RH variation for HBL with thickness $h_{NF} = 30 \mu\text{m}$, and

improvement can be exploited by sensor/actuator systems able to switch when the environmental conditions reach determined thresholds, as the carnivorous plant snaps when insects stimulate the trigger hair of the leaf.^[26] In this perspective, to demonstrate the usability of our HBS as part of an integrated system, we assembled an optical device based on the functionality of the bistable system. Exploiting the optical properties of PDMS, we fabricated a lens using drop casting technique^[31] and bonded it on the side of the HBS by plasma bonding activation, obtaining a bistable lens (Figure 3i). The bistable lens has been inserted in front of a collimated source of light to focus the beam on a point (Figure 3l), the environmental variation of RH allows the lens to suddenly snaps when a certain RH level is reached, moving the focus and allowing the focus/defocus of the laser beam on a target (Figure 3l-insets). The herein presented illustrative case study can be interpreted as a core switch of a more complex optical system. Thanks to the structural properties of this system, the application field of this approach is not limited just to the building of microdevices but can be of interest in each field in which energy efficiency is an issue. The integration of bistability and smart materials can be considered the building block in more complex systems able to rapidly reconfigure when particular environmental conditions manifest, leading to the assembly of advanced soft robotics systems. Let us remark that we pursued a bioinspired approach, in particular by deriving from the Venus flytrap the key physical phenomena allowing for snapping. Differently from the Venus flytrap leaf, however, we considered a surface with null Gaussian curvature (i.e., it can be distended over a plane without stretching/wrinkling), whereas the biological model features a nonzero Gaussian curvature. Strictly speaking, this would affect the snapping dynamics, yet the characteristic time for snapping does not substantially differ in between the biological model leaf and our artificial system. Indeed, we argue that the more complex geometry of the Venus flytrap leaf may be due to evolutionary pressure that optimized plant survival by improving its pray-catching ability also based on a caging leaf surface.^[21] From a functional viewpoint, also the proposed soft bistable structures can be optimized toward specific applications, for example renewable energy: the ability to harvest energy from the natural evaporation of water could be of interest where other energy sources are not available, especially for autonomous systems.^[32] Regarding the study limitations, the model-based approach we propose to study HBL should be extended to HBS by also modeling the snap-through energy barrier between the two stable states. The energetic barrier is strictly related to the value of the parameter \tilde{w} and it depends on the geometrical and elastic parameters of the system,^[22] while

the trigger of the snapping is related to the active layer capability to deform the bistable sheet. Also the constraints (mainly in terms of displacements in correspondence of holding components, yet load conditions would play a role as well) introduced by the specific embodiment affect the possibility for effectively snap. More refined approaches could be leveraged for a deeper investigation of the snapping conditions,^[33,34] however the herein presented approach emphasizes the importance of the synergy between structural and multifunctional properties of materials in soft systems, promoting the integration of environmentally responsive materials and smart structures in new soft devices and robots.

Experimental Section

Biological Investigation: Venus flytrap, *D. muscipula*, plants were grown in a growing chamber (AT 150 incubator, AMCOTA) at the CMBR center. Leaf samples were cut from healthy, adult plants. Thin strips were cut using razor blade to investigate the internal stress condition of the structure. Samples for microstructure investigation were processed using ethanol, embedded in wax, and cross-sections (10 μm thick) were cut through microtome (Leica SM2010R). Observations through polarized microscope were carried out by using a Nikon Eclipse Ni-U Upright microscope, interposing linear polarizing filters (LPVISE100-A and LPVISE200-A, Thorlabs) one perpendicular to each other on the optical path.

Bistable Device Fabrication: Silicon wafers (Si-Mat single side polished 380 μm thick) were silanized closing them in a Petri dish for 30 min with a cap containing a few drops of chlorotrimethylsilane (Sigma-Aldrich), used as silanizing agent. A film of PDMS (with 10:1 ratio of base to curing agent, Sylgard 184, Dow Corning Corp.) was spin-coated (SPS Europe Spin 150) at 600 rpm for 60 s and then cured in an oven at 100 °C for 60 min. Rectangular PDMS layers were cut using laser cut or razor blade and gently peeled off from the wafer using tweezers. Rectangular PDMS layers were then mounted on customized setups composed of micrometric sliders to control the axial deformation of each layer. Desired deformation was imposed and an oxygen plasma treatment (Gambetti Kenologia Colibri) was applied with a power of 30 W for 30 s. After the treatment, the prestressed rectangular PDMS layers were quickly brought in contact and pressed one on the other to create the bonding. After the bonding was produced, the sliders that were keeping the layers deformed were removed. As shown in 3 in the Supporting Information, no wrinkles were visible on the interface between the prestretched PDMS layers. The obtained bistable device was attached to the drum collector using paper tape and used as substrate for nanofibers deposition.

Electrospinning Nanofiber Deposition: PEO (300 000 g mol⁻¹, Sigma-Aldrich) was dissolved at a concentration of 10 wt% in deionized water and kept in agitation for two days on an orbital shaker at room temperature. The obtained homogenous solution was then electrospun through a syringe (25 G stainless steel). The collector-needle distance

d) curvature variation versus time induced by a step RH variation occurring at t_0 for a HBL with thicknesses $h_{\text{NF}} = 30$ and 60 μm . Both experimental data and model prediction are shown and saturation time to reach 90% of the regime (τ_{90}) is highlighted. e) Superposition of pictures showing the response of HBL during a RH variation cycle represented in (a), 1st and 100th cycles are shown (scale bar: 3 mm). f) Artificial Venus flytrap leaf (AVFL) obtained by laser cutting an HBS, based on the morphometry of the natural leaf (scale bar: 1 cm). g) AVFL mean normalized curvature variation in response to a humidity step variation from RH₁ to RH₂ (step large enough to cause the snap). The response time for curvature variation (τ_{snap}) is highlighted. h) The AVFL timescale for curvature variation (red triangles) is sensibly lower than the poroelastic limit $\tau = h_{\text{NF}}^2/D$ (dashed line), namely, the characteristic time for water to diffuse through the whole active layer. This confirms the instability-driven quick variation of the curvature for the AVFL. The diffusivity D was estimated based on the developed model. For completeness, the HBL timescales are also shown (blue squares) and they fall near the poroelastic limit, as expected. The gray band highlights the fact that the artificial leaf timescale is consistent with that one of the natural leaf (data reproduced from Skotheim^[14]). i) HBS integrating a preshaped PDMS dome to obtain a bistable focusing lens: schematic of the relevant manufacturing step, to be framed in the process shown in Figure 2. j) Illustrative focalization of a laser beam obtained when the bistable lens snaps (insets) in response to a change in relative humidity.

was imposed at 25 cm and the voltage applied to the polymer drop was 25 kV. The drum collector diameter was 8 cm and the rotational speed during the process was imposed to 2000 rpm. The drum collector was wrapped up with aluminum foil before the process.

NF Membrane and PDMS Film Morphology: NF membrane and PDMS spin-coated films thickness were measured through optical profilometer (Leica DCM 3D). NF membranes thickness were measured scratching the membrane electrospun on gold sputtered glass attached to the drum collector. PDMS spin-coated films were gold sputtered before optical profilometer measurements to avoid optical artifacts. Both measurements were compared with microscope measurements (Hirox KH 8700 Digital Microscope). SEM images of NF were obtained using FEI Helios NanoLab Dual Beam microscope (FEI Company: Hillsboro, OR, USA) by previously gold sputtering the samples.

NF Membrane Mechanical Characterization: NF electrospun membrane samples of 10 mm × 70 mm × 90 μm were cut using razor blade and gently peeled off from aluminum foil after electrospinning. Membrane samples were fixed using double-sided adhesive tape on stress-strain customized setup composed of ATI Nano 17 F/T Sensor and Physik Instrumente M-126 Precision Translation Stage. Tests were performed placing the setup in a climatic test chamber with controlled RH level at 25 °C. RH level and temperature were monitored using a SHT11 humidity and temperature sensor. Through the same setup, the hygroscopic expansion coefficient was measured as well, by monitoring the length variation of the samples when varying the RH level of the climatic chamber.

Bilayer PEO/PDMS Characterization: The responses of the bilayers were tested suddenly exposing a source of water in proximity to the devices and recording the response through webcam (Logitech C930e, 1080p resolution). RH level and temperature were monitored during the test through an SHT11 humidity and temperature sensor. Image processing analysis was manually performed to measure the curvature using ImageJ software.

Bistable Devices Characterization: Response times of bistable devices were measured recording through cameras (Canon EOS550D, Logitech C930e) and postprocessed with ImageJ software to measure the mean curvature of the system when abruptly exposed to a source of water.

Lens Fabrication: Planoconvex PDMS lens was fabricated following confined drop technique.^[31]

Supporting Information

Supporting Information is available from the Wiley Online Library or from the author.

Acknowledgements

The authors would like to acknowledge Cristina Ghelardi, Gabriella Meloni, and Andrea Degl'innocenti for assistance during the preparation of biological samples and for the fruitful discussions. The authors would also like to acknowledge Virgilio Mattoli for the support regarding the optical sources. This study was partially funded by the European Union's Horizon 2020 Research and Innovation Programme under Grant Agreement No. 824074 (GrowBot project).

Conflict of Interest

The authors declare no conflict of interest.

Keywords

bioinspiration, bistability, electrospinning, hygroscopic nanofibers, soft robots

Received: July 29, 2019

Revised: November 23, 2019

Published online: January 15, 2020

- [1] L. Hines, K. Petersen, G. Z. Lum, M. Sitti, *Adv. Mater.* **2017**, *29*, 1603483.
- [2] C. Majidi, *Adv. Mater. Technol.* **2019**, *4*, 1800477.
- [3] R. Yoshida, K. Uchida, Y. Kaneko, K. Sakai, A. Kikuchi, Y. Sakurai, T. Okano, *Nature* **1995**, *374*, 240.
- [4] O. M. Wani, H. Zeng, A. Priimagi, *Nat. Commun.* **2017**, *8*, 15546.
- [5] M. Ravi Shankar, M. L. Smith, V. P. Tondiglia, K. M. Lee, M. E. McConney, D. H. Wang, L. S. Tan, T. J. White, *Proc. Natl. Acad. Sci. USA* **2013**, *110*, 18792.
- [6] H. Chen, Y. Li, Y. Liu, T. Gong, L. Wang, S. Zhou, *Polym. Chem.* **2014**, *5*, 5168.
- [7] E. Reyssat, L. Mahadevan, *EPL* **2011**, *93*, 54001.
- [8] M. Ma, L. Guo, D. G. Anderson, R. Langer, *Science* **2013**, *339*, 186.
- [9] H. Lee, C. Xia, N. X. Fang, *Soft Matter* **2010**, *6*, 4342.
- [10] X. Chen, L. Mahadevan, A. Driks, O. Sahin, *Nat. Nanotechnol.* **2014**, *9*, 137.
- [11] J. Mu, C. Hou, H. Wang, Y. Li, Q. Zhang, M. Zhu, *Sci. Adv.* **2015**, *1*, e1500533.
- [12] S. Taccola, F. Greco, E. Sinibaldi, A. Mondini, B. Mazzolai, V. Mattoli, *Adv. Mater.* **2015**, *27*, 1668.
- [13] B. Shin, J. Ha, M. Lee, K. Park, G. H. Park, T. H. Choi, K. J. Cho, H.-Y. Kim, *Sci. Rob.* **2018**, *3*, eaar2629.
- [14] J. M. Skotheim, *Science* **2005**, *308*, 1308.
- [15] A. M. Manschadi, J. Christopher, P. deVoil, G. L. Hammer, *Funct. Plant Biol.* **2006**, *33*, 823.
- [16] I. Must, E. Sinibaldi, B. Mazzolai, *Nat. Commun.* **2019**, *10*, 344.
- [17] E. Reyssat, L. Mahadevan, *J. R. Soc., Interface* **2009**, *6*, 951.
- [18] R. Elbaum, L. Zaltzman, I. Burgert, P. Fratzl, *Science* **2007**, *316*, 884.
- [19] K. Oda, T. Abe, *Bot. Mag., Tokyo* **1972**, *85*, 135.
- [20] S. Poppinga, M. Joyeux, *Phys. Rev. E* **2011**, *84*, 041928.
- [21] C. Darwin, F. Darwin, *Insectivorous Plants*, John Murray, London **1888**.
- [22] Y. Forterre, J. M. Skotheim, J. Dumais, L. Mahadevan, *Nature* **2005**, *433*, 421.
- [23] D. Evangelista, S. Hotton, J. Dumais, *J. Exp. Biol.* **2011**, *214*, 521.
- [24] S. Armon, E. Efrati, R. Kupferman, E. Sharon, *Science* **2011**, *333*, 1726.
- [25] Y. Abraham, R. Elbaum, *New Phytol.* **2013**, *197*, 1012.
- [26] D. Hodick, A. Sievers, *Cell* **1982**, *320*, 95.
- [27] J. Mathew, Y. Semenova, G. Rajan, P. Wang, G. Farrell, *Opt. Laser Technol.* **2011**, *43*, 1301.
- [28] K. C. Tang, E. Liao, W. L. Ong, J. D. S. Wong, A. Agarwal, R. Nagarajan, L. Yobas, *J. Phys.: Conf. Ser.* **2006**, *34*, 155.
- [29] S. Timoshenko, *J. Opt. Soc. Am.* **1925**, *11*, 233.
- [30] M. Christophersen, B. Shapiro, E. Smela, *Sens. Actuators, B* **2006**, *115*, 596.
- [31] S. Ekgasit, N. Kaewmanee, P. Jangtawee, C. Thammacharoen, M. Donphoongpri, *ACS Appl. Mater. Interfaces* **2016**, *8*, 20474.
- [32] A. H. Cavusoglu, X. Chen, P. Gentine, O. Sahin, *Nat. Commun.* **2017**, *8*, 617.
- [33] N. A. Caruso, A. Cvetković, A. Lucantonio, G. Noselli, A. DeSimone, *Int. J. Mech. Sci.* **2018**, *149*, 481.
- [34] X. Jiang, M. Pezzulla, H. Shao, T. K. Ghosh, D. P. Holmes, *EPL* **2018**, *122*, 64003.